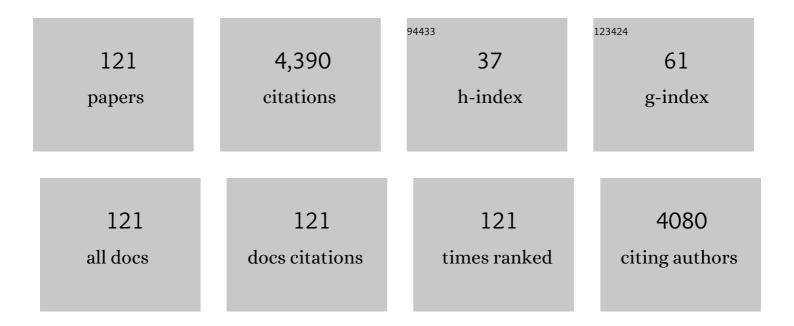
Zhaocong Wu

List of Publications by Year in descending order

Source: https://exaly.com/author-pdf/8270702/publications.pdf Version: 2024-02-01



#	Article	IF	CITATIONS
1	Land Surface Temperature Retrieval from Landsat 8 TIRS—Comparison between Radiative Transfer Equation-Based Method, Split Window Algorithm and Single Channel Method. Remote Sensing, 2014, 6, 9829-9852.	4.0	562
2	Visible and near-infrared reflectance spectroscopy—An alternative for monitoring soil contamination by heavy metals. Journal of Hazardous Materials, 2014, 265, 166-176.	12.4	265
3	Strategic assessment of the magnitude and impacts of sand mining in Poyang Lake, China. Regional Environmental Change, 2010, 10, 95-102.	2.9	165
4	Concurrent monitoring of vessels and water turbidity enhances the strength of evidence in remotely sensed dredging impact assessment. Water Research, 2007, 41, 3271-3280.	11.3	119
5	Methods and strategy for modeling daily global solar radiation with measured meteorological data – A case study in Nanchang station, China. Energy Conversion and Management, 2007, 48, 2447-2452.	9.2	112
6	Application of Sentinel 2 MSI Images to Retrieve Suspended Particulate Matter Concentrations in Poyang Lake. Remote Sensing, 2017, 9, 761.	4.0	107
7	Comparison of multivariate methods for estimating soil total nitrogen with visible/near-infrared spectroscopy. Plant and Soil, 2013, 366, 363-375.	3.7	100
8	A comparison of waveform processing algorithms for single-wavelength LiDAR bathymetry. ISPRS Journal of Photogrammetry and Remote Sensing, 2015, 101, 22-35.	11.1	97
9	Rapid urbanization and policy variation greatly drive ecological quality evolution in Guangdong-Hong Kong-Macau Greater Bay Area of China: A remote sensing perspective. Ecological Indicators, 2020, 115, 106373.	6.3	94
10	Estimation of arsenic in agricultural soils using hyperspectral vegetation indices of rice. Journal of Hazardous Materials, 2016, 308, 243-252.	12.4	84
11	Monitoring Arsenic Contamination in Agricultural Soils with Reflectance Spectroscopy of Rice Plants. Environmental Science & amp; Technology, 2014, 48, 6264-6272.	10.0	83
12	Spatiotemporal evolution of urban agglomerations in four major bay areas of US, China and Japan from 1987 to 2017: Evidence from remote sensing images. Science of the Total Environment, 2019, 671, 232-247.	8.0	80
13	Comparison of MODIS and Landsat TM5 images for mapping tempo–spatial dynamics of Secchi disk depths in Poyang Lake National Nature Reserve, China. International Journal of Remote Sensing, 2008, 29, 2183-2198.	2.9	75
14	Geo-detection of factors controlling spatial patterns of heavy metals in urban topsoil using multi-source data. Science of the Total Environment, 2018, 643, 451-459.	8.0	72
15	Thin cloud removal in optical remote sensing images based on generative adversarial networks and physical model of cloud distortion. ISPRS Journal of Photogrammetry and Remote Sensing, 2020, 166, 373-389.	11.1	69
16	Ensemble machine-learning-based framework for estimating total nitrogen concentration in water using drone-borne hyperspectral imagery of emergent plants: A case study in an arid oasis, NW China. Environmental Pollution, 2020, 266, 115412.	7.5	67
17	Greater flood risks in response to slowdown of tropical cyclones over the coast of China. Proceedings of the National Academy of Sciences of the United States of America, 2020, 117, 14751-14755.	7.1	67
18	Feasibility of estimating heavy metal concentrations in Phragmites australis using laboratory-based hyperspectral data—A case study along Le'an River, China. International Journal of Applied Earth Observation and Geoinformation, 2010, 12, S166-S170.	2.8	65

#	Article	IF	CITATIONS
19	A Scale-Synthesis Method for High Spatial Resolution Remote Sensing Image Segmentation. IEEE Transactions on Geoscience and Remote Sensing, 2012, 50, 4062-4070.	6.3	56
20	Soil Organic Carbon Content Estimation with Laboratory-Based Visible–Near-Infrared Reflectance Spectroscopy: Feature Selection. Applied Spectroscopy, 2014, 68, 831-837.	2.2	56
21	Improving Land Use/Land Cover Classification by Integrating Pixel Unmixing and Decision Tree Methods. Remote Sensing, 2017, 9, 1222.	4.0	56
22	Improving the prediction of arsenic contents in agricultural soils by combining the reflectance spectroscopy of soils and rice plants. International Journal of Applied Earth Observation and Geoinformation, 2016, 52, 95-103.	2.8	53
23	Mapping Tidal Flats with Landsat 8 Images and Google Earth Engine: A Case Study of the China's Eastern Coastal Zone circa 2015. Remote Sensing, 2019, 11, 924.	4.0	53
24	Using remotely sensed suspended sediment concentration variation to improve management of Poyang Lake, China. Lake and Reservoir Management, 2013, 29, 47-60.	1.3	51
25	Proximal and remote sensing techniques for mapping of soil contamination with heavy metals. Applied Spectroscopy Reviews, 2018, 53, 783-805.	6.7	51
26	New spectral metrics for mangrove forest identification. Remote Sensing Letters, 2016, 7, 885-894.	1.4	49
27	Improving satellite retrieval of oceanic particulate organic carbon concentrations using machine learning methods. Remote Sensing of Environment, 2021, 256, 112316.	11.0	49
28	Will the Three Gorges Dam affect the underwater light climate of VallisneriaÂspiralis L. and food habitat of Siberian crane in Poyang Lake?. Hydrobiologia, 2009, 623, 213-222.	2.0	47
29	Absorption and backscattering coefficients and their relations to water constituents of Poyang Lake, China. Applied Optics, 2011, 50, 6358.	2.1	45
30	Comparison of Machine Learning Techniques in Inferring Phytoplankton Size Classes. Remote Sensing, 2018, 10, 191.	4.0	44
31	Feasibility of estimating heavy metal contaminations in floodplain soils using laboratory-based hyperspectral data—A case study along Le'an River, China. Geo-Spatial Information Science, 2011, 14, 10-16.	5.3	42
32	Statistical model development and estimation of suspended particulate matter concentrations with Landsat 8 OLI images of Dongting Lake, China. International Journal of Remote Sensing, 2015, 36, 343-360.	2.9	42
33	An approach for developing Landsat-5 TM-based retrieval models of suspended particulate matter concentration with the assistance of MODIS. ISPRS Journal of Photogrammetry and Remote Sensing, 2013, 85, 84-92.	11.1	41
34	Comparison of MODIS-based models for retrieving suspended particulate matter concentrations in Poyang Lake, China. International Journal of Applied Earth Observation and Geoinformation, 2013, 24, 63-72.	2.8	39
35	Exploring Annual Urban Expansions in the Guangdong-Hong Kong-Macau Greater Bay Area: Spatiotemporal Features and Driving Factors in 1986–2017. Remote Sensing, 2020, 12, 2615.	4.0	39
36	Assessing toxic metal chromium in the soil in coal mining areas via proximal sensing: Prerequisites for land rehabilitation and sustainable development. Geoderma, 2022, 405, 115399.	5.1	39

#	Article	IF	CITATIONS
37	Performance of Landsat TM in ship detection in turbid waters. International Journal of Applied Earth Observation and Geoinformation, 2009, 11, 54-61.	2.8	38
38	A Wavelet-Based Area Parameter for Indirectly Estimating Copper Concentration in Carex Leaves from Canopy Reflectance. Remote Sensing, 2015, 7, 15340-15360.	4.0	38
39	A Spatially-Constrained Color–Texture Model for Hierarchical VHR Image Segmentation. IEEE Geoscience and Remote Sensing Letters, 2013, 10, 120-124.	3.1	37
40	Estimating Soil Organic Carbon Content with Visible–Near-Infrared (Vis-NIR) Spectroscopy. Applied Spectroscopy, 2014, 68, 712-722.	2.2	36
41	A Bilevel Scale-Sets Model for Hierarchical Representation of Large Remote Sensing Images. IEEE Transactions on Geoscience and Remote Sensing, 2016, 54, 7366-7377.	6.3	35
42	Wavelet-based coupling of leaf and canopy reflectance spectra to improve the estimation accuracy of foliar nitrogen concentration. Agricultural and Forest Meteorology, 2018, 248, 306-315.	4.8	33
43	Detecting Spatiotemporal Features and Rationalities of Urban Expansions within the Guangdong–Hong Kong–Macau Greater Bay Area of China from 1987 to 2017 Using Time-Series Landsat Images and Socioeconomic Data. Remote Sensing, 2019, 11, 2215.	4.0	33
44	Evaluating Different Methods for Grass Nutrient Estimation from Canopy Hyperspectral Reflectance. Remote Sensing, 2015, 7, 5901-5917.	4.0	31
45	Stepwise Evolution Analysis of the Region-Merging Segmentation for Scale Parameterization. IEEE Journal of Selected Topics in Applied Earth Observations and Remote Sensing, 2018, 11, 2461-2472.	4.9	31
46	Estimating leaf nitrogen concentration in heterogeneous crop plants from hyperspectral reflectance. International Journal of Remote Sensing, 2015, 36, 4652-4667.	2.9	29
47	Decomposition of LiDAR waveforms by B-spline-based modeling. ISPRS Journal of Photogrammetry and Remote Sensing, 2017, 128, 182-191.	11.1	28
48	Mapping invasive plant with UAV-derived 3D mesh model in mountain area—A case study in Shenzhen Coast, China. International Journal of Applied Earth Observation and Geoinformation, 2019, 77, 129-139.	2.8	28
49	Digital mapping of zinc in urban topsoil using multisource geospatial data and random forest. Science of the Total Environment, 2021, 792, 148455.	8.0	28
50	Rapid Urbanization Induced Extensive Forest Loss to Urban Land in the Guangdong-Hong Kong-Macao Greater Bay Area, China. Chinese Geographical Science, 2021, 31, 93-108.	3.0	28
51	Monitoring the impact of backflow and dredging on water clarity using MODIS images of Poyang Lake, China. Hydrological Processes, 2009, 23, 342-350.	2.6	27
52	Understanding Seasonal Water Clarity Dynamics of Lake Dahuchi from In Situ and Remote Sensing Data. Water Resources Management, 2009, 23, 1849-1861.	3.9	27
53	Developing MODIS-based retrieval models of suspended particulate matter concentration in Dongting Lake, China. International Journal of Applied Earth Observation and Geoinformation, 2014, 32, 46-53.	2.8	27
54	Successive projections algorithm-based three-band vegetation index for foliar phosphorus estimation. Ecological Indicators, 2016, 67, 12-20.	6.3	27

#	Article	IF	CITATIONS
55	CCANet: Class-Constraint Coarse-to-Fine Attentional Deep Network for Subdecimeter Aerial Image Semantic Segmentation. IEEE Transactions on Geoscience and Remote Sensing, 2022, 60, 1-20.	6.3	27
56	Small water bodies mapped from Sentinel-2 MSI (MultiSpectral Imager) imagery with higher accuracy. International Journal of Remote Sensing, 2020, 41, 7912-7930.	2.9	26
57	Determining switching threshold for NIR-SWIR combined atmospheric correction algorithm of ocean color remote sensing. ISPRS Journal of Photogrammetry and Remote Sensing, 2019, 153, 59-73.	11.1	25
58	Unsupervised Simplification of Image Hierarchies via Evolution Analysis in Scale-Sets Framework. IEEE Transactions on Image Processing, 2017, 26, 2394-2407.	9.8	23
59	Improving Spectral Estimation of Soil Organic Carbon Content through Semi-Supervised Regression. Remote Sensing, 2017, 9, 29.	4.0	23
60	Self-Attentive Generative Adversarial Network for Cloud Detection in High Resolution Remote Sensing Images. IEEE Geoscience and Remote Sensing Letters, 2020, 17, 1792-1796.	3.1	23
61	Newly-developed three-band hyperspectral vegetation index for estimating leaf relative chlorophyll content of mangrove under different severities of pest and disease. Ecological Indicators, 2022, 140, 108978.	6.3	23
62	Assessing spatiotemporal variations and predicting changes in ecosystem service values in the Guangdong–Hong Kong–Macao Greater Bay Area. GIScience and Remote Sensing, 2022, 59, 184-199.	5.9	21
63	Spectroscopic Diagnosis of Arsenic Contamination in Agricultural Soils. Sensors, 2017, 17, 1036.	3.8	20
64	Continuous Wavelet Analysis of Leaf Reflectance Improves Classification Accuracy of Mangrove Species. Remote Sensing, 2019, 11, 254.	4.0	20
65	Deep Learning Based Thin Cloud Removal Fusing Vegetation Red Edge and Short Wave Infrared Spectral Information for Sentinel-2A Imagery. Remote Sensing, 2021, 13, 157.	4.0	20
66	Comparison of Satellite-Derived Phytoplankton Size Classes Using In-Situ Measurements in the South China Sea. Remote Sensing, 2018, 10, 526.	4.0	18
67	Simulating and forecasting spatio-temporal characteristic of land-use/cover change with numerical model and remote sensing: a case study in Fuxian Lake Basin, China. European Journal of Remote Sensing, 2019, 52, 374-384.	3.5	18
68	Mapping lead concentrations in urban topsoil using proximal and remote sensing data and hybrid statistical approaches. Environmental Pollution, 2021, 272, 116041.	7.5	18
69	A Lightweight Deep Learning-Based Cloud Detection Method for Sentinel-2A Imagery Fusing Multiscale Spectral and Spatial Features. IEEE Transactions on Geoscience and Remote Sensing, 2022, 60, 1-19.	6.3	18
70	Mapping Aquaculture Areas with Multi-Source Spectral and Texture Features: A Case Study in the Pearl River Basin (Guangdong), China. Remote Sensing, 2021, 13, 4320.	4.0	18
71	The Impacts of Building Orientation on Polarimetric Orientation Angle Estimation and Model-Based Decomposition for Multilook Polarimetric SAR Data in Urban Areas. IEEE Transactions on Geoscience and Remote Sensing, 2016, 54, 5520-5532.	6.3	16
72	Mapping leaf chlorophyll content of mangrove forests with Sentinel-2 images of four periods. International Journal of Applied Earth Observation and Geoinformation, 2021, 102, 102387.	2.8	16

#	Article	IF	CITATIONS
73	Reflectance spectroscopy for assessing heavy metal pollution indices in mangrove sediments using XGBoost method and physicochemical properties. Catena, 2022, 211, 105967.	5.0	16
74	Representation of Block-Based Image Features in a Multi-Scale Framework for Built-Up Area Detection. Remote Sensing, 2016, 8, 155.	4.0	15
75	Evaluating the effectiveness of the pollutant discharge permit program in China: A case study of the Nenjiang River Basin. Journal of Environmental Management, 2019, 251, 109501.	7.8	14
76	Uncertainty analysis of object location in multi-source remote sensing imagery classification. International Journal of Remote Sensing, 2009, 30, 5473-5487.	2.9	13
77	Spatial-Temporal Analysis and Stability Investigation of Coastline Changes: A Case Study in Shenzhen, China. IEEE Journal of Selected Topics in Applied Earth Observations and Remote Sensing, 2018, 11, 45-56.	4.9	13
78	Exploring Impact of Spatial Unit on Urban Land Use Mapping with Multisource Data. Remote Sensing, 2020, 12, 3597.	4.0	13
79	Spatiotemporal characteristics of land degradation in the Fuxian Lake Basin, China: Past and future. Land Degradation and Development, 2020, 31, 2446-2460.	3.9	13
80	The integration of species information and soil properties for hyperspectral estimation of leaf biochemical parameters in mangrove forest. Ecological Indicators, 2020, 115, 106467.	6.3	12
81	Estimating ultraviolet reflectance from visible bands in ocean colour remote sensing. Remote Sensing of Environment, 2021, 258, 112404.	11.0	12
82	Comparison of extrapolation and interpolation methods for estimating daily photosynthetically active radiation (PAR). Geo-Spatial Information Science, 2010, 13, 235-242.	5.3	11
83	Emotional habitat: mapping the global geographic distribution of human emotion with physical environmental factors using a species distribution model. International Journal of Geographical Information Science, 2021, 35, 227-249.	4.8	11
84	Bias Compensation for Rational Polynomial Coefficients of High-Resolution Satellite Imagery by Local Polynomial Modeling. Remote Sensing, 2017, 9, 200.	4.0	10
85	Comparing hillside urbanizations of Beijing-Tianjin-Hebei, Yangtze River Delta and Guangdong–Hong Kong–Macau greater Bay area urban agglomerations in China. International Journal of Applied Earth Observation and Geoinformation, 2021, 102, 102460.	2.8	10
86	Specific absorption and backscattering coefficients of the main water constituents in Poyang Lake, China. Environmental Monitoring and Assessment, 2013, 185, 4191-4206.	2.7	9
87	Mitigation of Reflection Symmetry Assumption and Negative Power Problems for the Model-Based Decomposition. IEEE Transactions on Geoscience and Remote Sensing, 2016, 54, 7261-7271.	6.3	9
88	Revisiting effectiveness of turbidity index for the switching scheme of NIR-SWIR combined ocean color atmospheric correction algorithm. International Journal of Applied Earth Observation and Geoinformation, 2019, 76, 1-9.	2.8	9
89	Characteristics and trends of hillside urbanization in China from 2007 to 2017. Habitat International, 2022, 120, 102502.	5.8	9
90	Small Water Body Detection and Water Quality Variations with Changing Human Activity Intensity in Wuhan. Remote Sensing, 2022, 14, 200.	4.0	9

#	Article	IF	CITATIONS
91	Analysis of Coastline Changes and the Socio-economic Driving Mechanisms in Shenzhen, China. Marine Geodesy, 2017, 40, 378-403.	2.0	8
92	Evolution of Frequency and Intensity of Concurrent Heavy Precipitation and Storm Surge at the Global Scale: Implications for Compound Floods. Frontiers in Earth Science, 2021, 9, .	1.8	8
93	Evaluation of Ocean Color Atmospheric Correction Methods for Sentinel-3 OLCI Using Global Automatic <i>In Situ</i> Observations. IEEE Transactions on Geoscience and Remote Sensing, 2022, 60, 1-19.	6.3	8
94	Research on remote sensing image classification using neural network based on rough sets. , 0, , .		7
95	A MODIS-Based Retrieval Model of Suspended Particulate Matter Concentration for the Two Largest Freshwater Lakes in China. Sustainability, 2016, 8, 832.	3.2	7
96	Adaptive Two-Component Model-Based Decomposition for Polarimetric SAR Data Without Assumption of Reflection Symmetry. IEEE Transactions on Geoscience and Remote Sensing, 2017, 55, 197-211.	6.3	7
97	An enhanced approach for surface flow routing over drainageâ€constrained triangulated irregular networks. Transactions in GIS, 2018, 22, 43-57.	2.3	7
98	Developing Growth Models of Stand Volume for Subtropical Forests in Karst Areas: A Case Study in the Guizhou Plateau. Forests, 2021, 12, 83.	2.1	6
99	Monitoring variation of water turbidity and related environmental factors in Poyang Lake National Nature Reserve, China. , 2007, , .		5
100	GPU ray casting method for visualizing 3D pipelines in a virtual globe. International Journal of Digital Earth, 2019, 12, 428-441.	3.9	5
101	Extreme Phytoplankton Blooms in the Southern Tropical Indian Ocean in 2011. Journal of Geophysical Research: Oceans, 2020, 125, e2019JC015649.	2.6	5
102	High-Frequency Variations in Pearl River Plume Observed by Soil Moisture Active Passive Sea Surface Salinity. Remote Sensing, 2020, 12, 563.	4.0	5
103	A Fast and Robust Scan-Line Search Algorithm for Object-to-Image Projection of Airborne Pushbroom Images. Photogrammetric Engineering and Remote Sensing, 2015, 81, 565-572.	0.6	4
104	Trajectory Data Mining via Cluster Analyses for Tropical Cyclones That Affect the South China Sea. ISPRS International Journal of Geo-Information, 2017, 6, 210.	2.9	4
105	Scale-sets image classification with hierarchical sample enriching and automatic scale selection. International Journal of Applied Earth Observation and Geoinformation, 2021, 105, 102605.	2.8	4
106	EstimatingCarexquality with laboratory-based hyperspectral measurements. International Journal of Remote Sensing, 2013, 34, 1866-1878.	2.9	3
107	A GIS Study of the Influences of Warm Ocean Eddies on the Intensity Variations of Tropical Cyclones in the South China Sea. ISPRS International Journal of Geo-Information, 2016, 5, 169.	2.9	3
108	Hierarchical Segmentation Evaluation of Region-Based Image Hierarchy. IEEE Journal of Selected Topics in Applied Earth Observations and Remote Sensing, 2019, 12, 2718-2727.	4.9	3

#	Article	IF	CITATIONS
109	Spatiotemporal dynamics of forest ecosystem carbon budget in Guizhou: customisation and application of the CBM-CFS3 model for China. Carbon Balance and Management, 2022, 17, .	3.2	3
110	Marker-based watershed segmentation embedded with edge information. , 2010, , .		2
111	A Glimpse of Ocean Color Remote Sensing From Moon-Based Earth Observations. IEEE Transactions on Geoscience and Remote Sensing, 2022, 60, 1-11.	6.3	2
112	A review of remote-sensing-based spatial/temporal information capturing for water resource studies in Poyang Lake. Proceedings of SPIE, 2009, , .	0.8	1
113	Study on the relationship between aerosol anthropogenic component and air quality in the city of Wuhan. , 2011, , .		1
114	Gross primary production estimation by combining MODIS products and Ameriflux data through Artificial Neural Network for croplands. , 2012, , .		1
115	Investigating the potential of GIMMS and MODIS NDVI data sets for estimating gross primary productivity in Harvard Forest. , 2013, , .		1
116	Response to "Visible and near-infrared reflectance spectroscopy is of limited practical use to monitor soil contamination by heavy metals―by Philippe C. Baveye. Journal of Hazardous Materials, 2015, 285, 207.	12.4	1
117	A Highly Efficient Method for Training Sample Selection in Remote Sensing Classification. , 2018, , .		1
118	Selection of Optimal Bands for Hyperspectral Local Feature Descriptor. IEEE Geoscience and Remote Sensing Letters, 2022, 19, 1-5.	3.1	1
119	Seasonal changes of the relationships between photochemical reflectance index and light use efficiency in broadleaf forest. , 2010, , .		0
120	Feasibility of estimating heavy metal concentrations in wetland soil using hyperspectral technology. , 2017, , .		0
121	ROUGH SET BASED FEATURE SELECTION FOR CLASSIFICATION OF HIGH SPATIAL RESOLUTION REMOTE SENSING IMAGERY. , 2010, , .		0